fire

MDPI

Article

Numerical Analysis of Smoke Behavior and Detection of Solid Combustible Fire Developed in Manned Exploration Module Based on Exploration Gravity

Ter-Ki Hong [1] and Seul-Hyun Park [2,*]

[1] Department of Mechanical System & Automotive Engineering, Graduate School of Chosun University, 309 Pilmum-daero, Dong-gu, Gwangju 61452, Korea; catzeyeh@chosun.kr
[2] Department of Mechanical Engineering, Chosun University, 309 Pilmum-daero, Dong-gu, Gwangju 61452, Korea
* Correspondence: isaac@chosun.ac.kr; Tel.: +82-62-230-7174; Fax: +82-62-230-7171

Abstract: A fire during manned space exploration can cause serious casualties and disrupt the mission if the initial response is delayed. Therefore, measurement technology that can detect fire in the early stage of ignition is important. There have been a number of works that investigate the smoke behaviors in microgravity as the foundation for a reliable method for sensing a fire during spaceflight. For space missions to the outer planets, however, a strategy of detecting smoke as an indicator of fire should be adjusted to cover the fire scenario that can be greatly affected by changes in gravity (microgravity, lunar, Mars, and Earth gravity). Therefore, as a preliminary study on fire detectors of the manned pressurized module, the present study examined the smoke particle behavior and detection characteristics with respect to changes in gravity using numerical analysis. In particular, the effects of the combination of buoyancy and ventilation flow on the smoke particle movement pattern was investigated to further improve the understanding of the fire detection characteristics of the smoke detector, assuming that a fire occurred in different gravity environments inside the pressurized module. To this end, we modeled the internal shape of Destiny and performed a series of numerical analysis using the Fire Dynamics Simulator (FDS). The findings of this study can provide basic data for the design of a fire detection system for manned space exploration modules.

Keywords: international space station; Fire Dynamics Simulator; smoke detector; space fire

Citation: Hong, T.-K.; Park, S.-H. Numerical Analysis of Smoke Behavior and Detection of Solid Combustible Fire Developed in Manned Exploration Module Based on Exploration Gravity. *Fire* **2021**, *4*, 85. https://doi.org/10.3390/fire4040085

Academic Editor: Wojciech Węgrzyński

Received: 15 October 2021
Accepted: 17 November 2021
Published: 19 November 2021

1. Introduction

In the history of space development, the fire incident [1] that occurred during the final ground experiment of Apollo 1 in 1967 has been recorded as a major accident that took the lives of all the crew on board. The fire accident [2] that occurred in the Russian manned space station Mir did not cause casualties but could lead to significant damage because it was in actual operation in orbit. Both fire accidents were related to the atmospheric environment inside the pressurized module. Thus, a system that can quickly detect and suppress fires must be included in the design of the Environmental Control and Life Support System (ECLSS) for the manned exploration pressurized module. In particular, if an early response is delayed in the event of a fire in a manned exploration module, it can cause not only casualties but also a major hindrance to the mission. Therefore, a technology to detect fire quickly in the early stage of ignition and a protocol for fire suppression must be established.

Constructed under the initiative of NASA, the European Space Agency, and the Japan Aerospace Exploration Agency after the fire incident on Mir, the ISS has installed a photoelectric smoke detector, which generates fire alarm signals by detecting smoke particles optically, inside the pressurized module. Urban et al. [3] numerically analyzed the detection time of photoelectric smoke detectors with respect to the smoke yield by

modeling the ISS Destiny Laboratory Module and assuming smoke particles generated from the burning of combustibles in a microgravity environment as soot. They reported that the fire detection time of smoke detectors can change greatly depending on the change of soot yield, and fire may not be detected depending on the position of the detector and the flow pattern when the soot yield is lower than 0.05.

In the microgravity environment, the movements of particles by buoyancy during a fire are highly limited as the effect of the buoyancy-driven flow disappears. Therefore, to detect fire using photoelectric smoke detectors, the design of ventilation flow that can move smoke particles is crucial. Brooker et al. [4] researched the fire detection characteristics of the photoelectric smoke detector with respect to the pattern of inter-module ventilation (IMV) flow in a microgravity environment for the ISS Destiny Laboratory Module, and they found that the fire detection time can be shortened by adding the IMV flow to the given ventilation flow condition. Unlike the ISS Destiny Laboratory Module under microgravity, the pressurized module to be used in the exploration of the Moon and Mars has different effects of flow governed by buoyancy in the event of fire depending on the change in gravity, which can eventually alter the residence time for fuel and species transports [5]. In particular, the change in residence time is a factor that controls the time required for the nucleation and growth of smoke particles and thus can significantly affect the concentration and optical properties of smoke generated by fire. Since changes in the concentration and optical properties of smoke can directly affect the light scattering and absorption characteristics of the particles [6,7], they can influence the operation characteristics of the photoelectric smoke detector installed inside the manned exploration module as reported in previous studies [8,9]. Recently, there have been extensive studies [10–13] on the morphological and optical properties of smoke particles produced from microgravity combustion. These studies demonstrated that the performance of photoelectric fire detectors can be varied with changes in morphological and optical properties of smoke particles influenced by extended duration of residence time in microgravity.

However, as examined above, existing research on fire detection systems in manned exploration modules has been limited to the microgravity environment. Therefore, as a preliminary study on fire detectors of the manned pressurized module, the present study examined the smoke particle behavior and detection characteristics with respect to changes in gravity (microgravity, lunar, Mars, and Earth gravity) using numerical analysis. In particular, we examined the effects of the combination of buoyancy and ventilation flow on the smoke particle movement pattern and investigated the fire detection characteristics of the smoke detector, assuming that a fire occurred in different gravity environments inside the pressurized module. To this end, we modeled the internal shape of Destiny, of which the internal shape and ventilation flow conditions of the pressurized module are well known, and performed a series of numerical analyses using the Fire Dynamics Simulator (FDS) developed by the National Institute of Standards and Technology (NIST) of the d States.

2. Materials and Methods

2.1. Determination of Combustion and Thermal Properties of ABS and PVC

To simulate a real fire in the manned pressurized module, we selected ABS, which is often used as a material for PCs or monitors, and PVC, which is used as a material for electric wires, as combustibles (fuels). In particular, PVC was selected to quantify the effect of smoke yield on the smoke detector operation because it generates less smoke during combustion than ABS [14,15]. Since the FDS numerical analysis requires the combustion characteristics of ABS and PVC fuels such as mass loss rate (MLR), smoke (soot) and CO yields, and effective heat of combustion, the ISO 5660-1 cone calorimetry experiment [16] was conducted. More details on the ISO 5660-1 cone calorimetry experiment can be found elsewhere [17].

ABS and PVC samples of 10 mm thickness were cut to a size of 100 (W) × 100 (L) and fixed to the sample holder as shown in Figure 1. They were then ignited spontaneously by applying a radiant heat flux of 50 kW/m^2 to the sample surface using a cone heater. The experiment was terminated by observing the extinction of the flame and no change in mass. Figure 2a displays the measured fuel MLR from the cone calorimetry experiments as a function of time. As shown in the figure, the mass reduction rates of PVC and ABS increased sharply after ignition and reached the quasi-steady state before decreasing with the extinction of flame. After measuring the mass loss from t_1 to t_2 of the quasi-steady section, the average fuel MLR was calculated using the following Equation (1):

$$\overline{\dot{m}}_f = \frac{\Delta m_f}{(t_2 - t_1)} \tag{1}$$

Figure 2b shows a graph of the CO yield calculated using the CO production rate and fuel MLR measured in real time during the burning of ABS and PVC in the cone calorimetry experiment. After calculating the time-averaged CO production rate ($\overline{\dot{m}}_{CO}$) and the average fuel MLR ($\overline{\dot{m}}_f$) in the quasi-steady section in the figure, the CO yield (y_{CO}) for each fuel was obtained using Equation (2). As illustrated in Figure 2, the CO yield generated during the burning of ABS was approximately twice that during the burning of PVC.

$$y_{CO} = \frac{\overline{\dot{m}}_{CO}}{\overline{\dot{m}}_f} \tag{2}$$

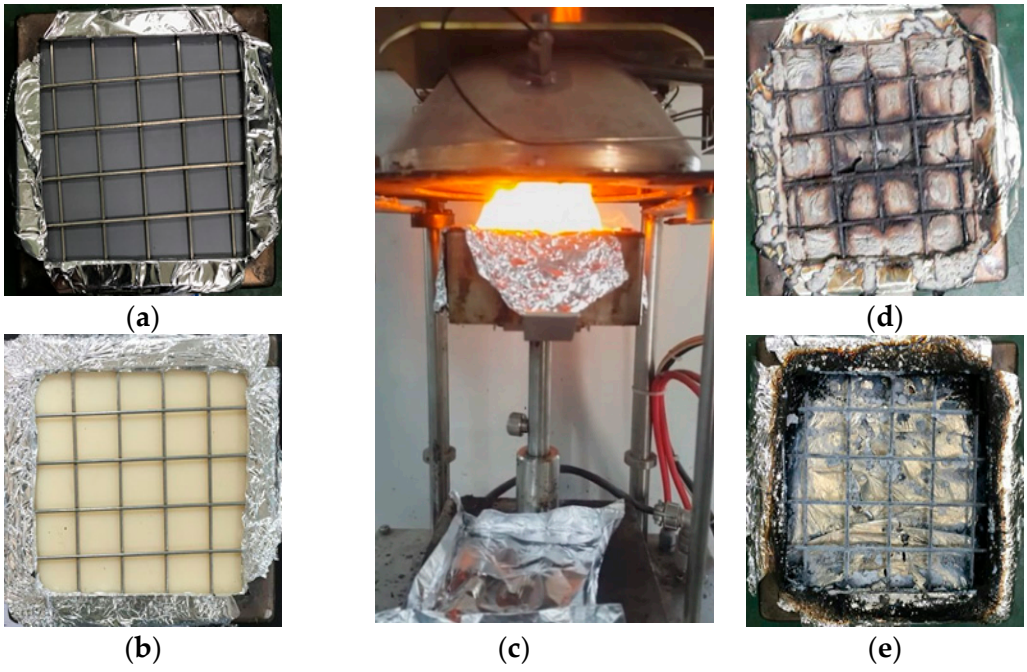

Figure 1. Burning experiments of ABS and PVC with ISO 5660-1 cone calorimeter: (**a**) PVC before experiment; (**b**) ABS before experiment; (**c**) Cone calorimeter experiment; (**d**) PVC after experiment; (**e**) ABS after experiment.

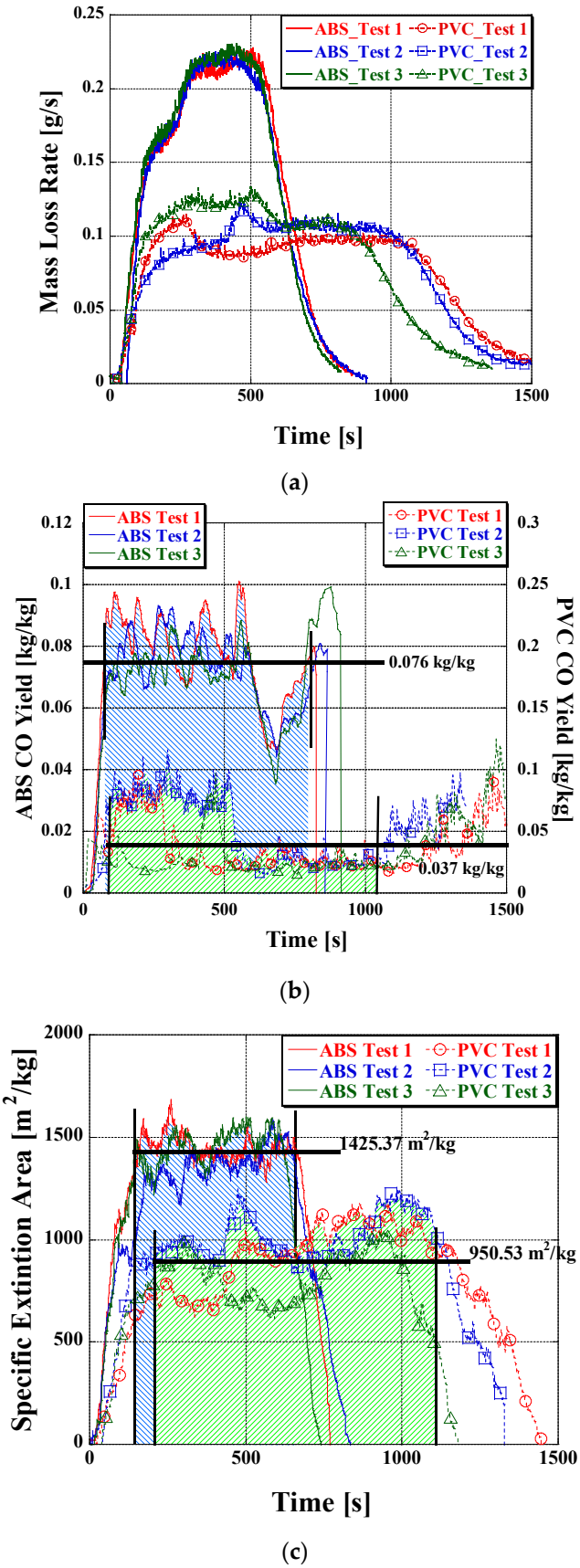

Figure 2. Cone calorimeter results as a function of time: (**a**) mass-loss rate; (**b**) CO yield; (**c**) specific extinction area.

The specific extinction area (SEA) by smoke particles can be obtained from the correlation between the light extinction coefficient (k) measured using the laser and photodiode installed in the duct above the cone calorimeter and the fuel MLR ($\overline{\dot{m}}_f$) (Equation (3) [18]. Figure 2c shows a graph of the SEA calculated using Equation (3) as a function of time. The soot yield (y_{Soot}) can be then calculated using Equation (4) as a ratio of the SEA and mass extinction coefficient (k_m). In this study, the k_m values use for ABS and PVC smoke particles were 7.8 m^2/g and 4.5 m^2/g, respectively, based on the reference [19].

$$\text{SEA} = \frac{kv_{duct,}}{\overline{\dot{m}}_f} \tag{3}$$

$$y_{Soot} = \frac{\text{SEA}}{k_m} = \frac{\overline{\dot{m}}_{soot}}{\overline{\dot{m}}_f} \tag{4}$$

Table 1 summarizes the result of the soot and CO yields and effective heat of combustion obtained from the cone calorimetry experiment of ABS and PVC. As listed in Table 1, the soot yield of PVC was lower than that of ABS. PVC is a flame-retardant polymer that suppresses heat release from flames owing to the high content of chlorine [20,21] and the smoke generation rate decreases with the flame.

Table 1. Summary of soot and CO yields and effective heat of combustion for ABS and PVC combustibles.

	ABS			**PVC**		
	Soot Yield, y_{Soot}	CO Yield, y_{CO}	Effective Heat of Combustion, ΔH_e (MJ/kg)	Soot Yield, y_{Soot}	CO Yield, y_{CO}	Effective Heat of Combustion, ΔH_e (MJ/kg)
Average	0.156	0.076	79.47	0.105	0.037	77.31

2.2. FDS Numrical Anaysiss

To examine the smoke particle behavior and detection characteristics with respect to the change in gravity (microgravity, lunar gravity, and Mars gravity), the ISS Destiny module of the NASA was modeled using FDS (Version 6.7.1). FDS is a hydrodynamic model that can be used to numerically solve the form of the Navier–Stokes equation for low-speed heat flow focused on the transfer of smoke and heat caused by fire [22]. The Large Eddy Simulation (LES) is used to calculate the flow and separates the instantaneous physical quantity into large-scale and sub-grid scale eddy through spatial filtering. More details on FDS are well documented in references [22,23].

Figure 3 shows the internal shape of the ISS Destiny module modeled based on a reference [4]. It is composed of 282,240 cells with a grid length of 0.05 m in total in a space of 8 (W) × 2.1 (L) × 2.1 (H) m. The inside of the Destiny module is composed of experimental modules of 24 International Standard Payload Racks (6 racks on each wall). As shown in Figure 3, there is a diffuser and a register between the modules. In particular, the IMV installed at the bottom of the hatch of the module is designed to help ventilation between ISS pressurized modules. The gravitational accelerations based on gravity change were input for microgravity (0 m/s^2) and lunar (1.62 m/s^2), Mars (3.71 m/s^2), and Earth (9.81 m/s^2) gravities.

Table 2 shows the boundary conditions for each ventilation type based on references [3,24] considering the working environment for the flow rates of diffuser, register, hatch, and IMV diffuser of a real ISS Destiny module. As shown in Figure 3, 6 photoelectric smoke detectors which generate fire alarm signals by optically detecting smoke particles. are installed in each return register.

A fire was numerically simulated by imposing a designed Heat Release Rate (HRR) on an area of 0.01 m^2 as combustibles at the center of the module. The HRR per unit area, $\dot{q}''$, generated from the ignited combustible gas can be determined using the MLR and effective

heat of combustion, ΔH_e, for ABS/PVC obtained from the cone calorimetry experiments as follows:

$$\dot{q}'' = \dot{m}'' \Delta H_e \tag{5}$$

For the combustion reaction, FDS uses the mixing-controlled combustion model based on the eddy dissipation concept, which is controlled by the characteristic mixing time of fuel/air under the infinitely fast reaction of fuel/air. The combustion reactions of each of fuel, i.e., ABS and PVC, along with the yields of CO and soot were defined as follows:

$$\begin{aligned} \text{ABS} : \underbrace{1(C_{15}H_{17}N)}_{Fuel} & + \underbrace{16.168678}_{v_{air}}\underbrace{(O_2 + 3.76N_2)}_{air} \\ & \rightarrow 1\left(\underbrace{11.707546}_{v_{CO_2}}CO_2 + \underbrace{0.573328}_{v_{CO}}CO + \underbrace{8.348937}_{v_{H_2O}}H_2O \right. \\ & \left. + \underbrace{16.301657}_{v_{N_2}}(3.76)N_2\right) + \underbrace{3.021252}_{v_{Soot}}\underbrace{C_{0.9}H_{0.1}\text{Soot}}_{Soot} \end{aligned} \tag{6}$$

$$\begin{aligned} \text{PVC} : \underbrace{1(C_2H_3Cl)}_{Fuel} & + \underbrace{1.90236}_{v_{air}}\underbrace{(O_2 + 3.76N_2)}_{air} \\ & \rightarrow 1\left(\underbrace{1}_{v_{HCl}}HCl + \underbrace{1.376118}_{v_{CO_2}}CO_2 + \underbrace{0.08255715}_{v_{CO}}CO \right. \\ & \left. + \underbrace{0.9699264}_{v_{H_2O}}H_2O + \underbrace{1.90236(3.76)}_{v_{N_2}}N_2\right) \\ & + \underbrace{0.6014719}_{v_{Soot}}\underbrace{C_{0.9}H_{0.1}\text{Soot}}_{Soot} \end{aligned} \tag{7}$$

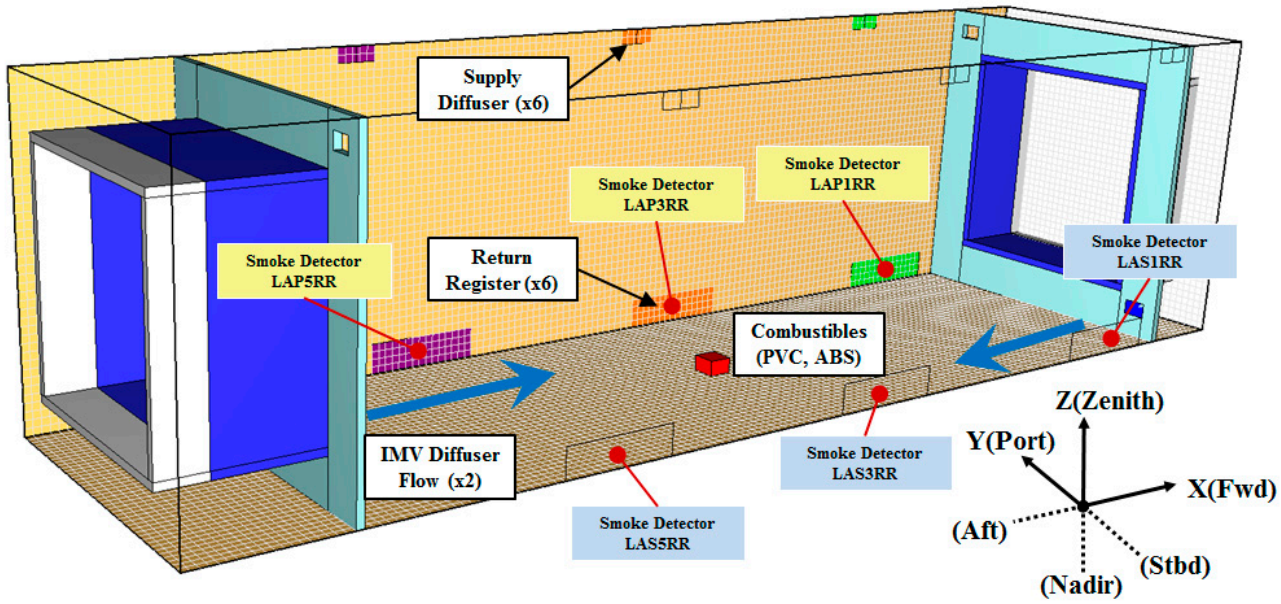

Figure 3. ISS Destiny Laboratory model showing main section, endcones, and hatches enclosed within a rectilinear grid. There are six overhead supply diffusers, six deck return registers, and one aft-port IMV diffuser for air ventilation. Induced flow patterns are indicated with lines.

Table 2. Summary of boundary conditions for each ventilation type [3,24].

Ventilation Type (Location)	Quantity	Boundary Condition		
		Type	Flow Rate (m^3/s)	Velocity Vector (m/s) (x, y, z)
Starboard Supply Air Diffuser (Left upper side on x–z plane)	3	Inlet	0.024	(±0.358, +0.620, −0.261)
Port Supply Air Diffuser (Right upper side on x–z plane)	3	Inlet	0.024	(±0.130, −0.226, −0.716)
Starboard Return Register (Left lower side on x–z plane)	3	Outlet	0.024	(0.0, +0.194, −0.194)
Port Return register (Right lower side on x–z plane)	3	Outlet	0.024	(0.0, −0.194, −0.194)
Aft and Fwd IMV diffuser (Both side ends below hatch)	2	Inlet	0.057	(±3.25, 0.0, 0.0)
Aft and Fwd IMV Register (Both side ends below hatch)	2	Outlet	0.057	Pressure Outlet

In the reactions, soot (i.e., smoke particles) is assumed to consist of carbon and hydrogen atoms, and the fraction of hydrogen atoms in soot was assigned to 0.1 in Equation (8) [23] as follows:

$$m_{Soot} = X_H \cdot m_H + (1 - X_H) \cdot m_c \tag{8}$$

where X_H is the fraction of hydrogen atoms in soot, m_{Soot} is the molar mass of soot, m_H is the molar mass of hydrogen, and m_c is the molar mass of hydrogen. The stochiometric coefficients for CO, v_{CO}, and soot, v_{Soot}, were then calculated using the measured average yields of CO (y_{CO}) and soot (y_{Soot}) listed in Table 1 as follows:

$$v_{CO} = \frac{m_F}{m_{CO}} \cdot y_{CO}; \;\; v_{Soot} = \frac{m_F}{m_{Soot}} \cdot y_{Soot} \tag{9}$$

The stochiometric coefficients for the other species in Equations (6) and (7) were eventually determined by arranging atomic balances.

In FDS calculations based on LES, determining the nominal size of the mesh cell, dx, and the characteristic fire diameter, D^*, is important to resolve the fluid flow and fire dynamics [23] as follows:

$$D^* = \left(\frac{\dot{Q}}{\rho_\infty c_p T_\infty \sqrt{g}} \right)^{\frac{2}{5}} \tag{10}$$

where $\dot{Q}$ is the fire HRR (kW), ρ_∞ is the ambient density of air (kg/m^3), c_p is the specific heat of air (kJ/kg·K), T_∞ is the ambient air temperature (K), and g is the acceleration of gravity (m/s^2). The ratio D*/dx between 4 and 16 can be taken as an adequate number of computational cells spanning the characteristic diameter of the fire developed in Earth gravity [24]. In the present study, the nominal size of mesh cell, dx, was varied from relatively coarse (5 cm) to fine mesh (2 cm) to investigate the effect of different cell sizes on predicting the soot mass fraction (which is a critical factor for evaluating the smoke detection time). As illustrated in Figure 4, the soot mass fraction calculated at the location of smoke detector, LAS3RR, was not dependent on the resolution of the mesh below dx of 5 cm, which corresponds to a D^*/dx ratio of 4.2 both in Earth and microgravity conditions. Therefore, 5 cm was considered as an appropriate cell size for all complementary simulations provided hereafter.

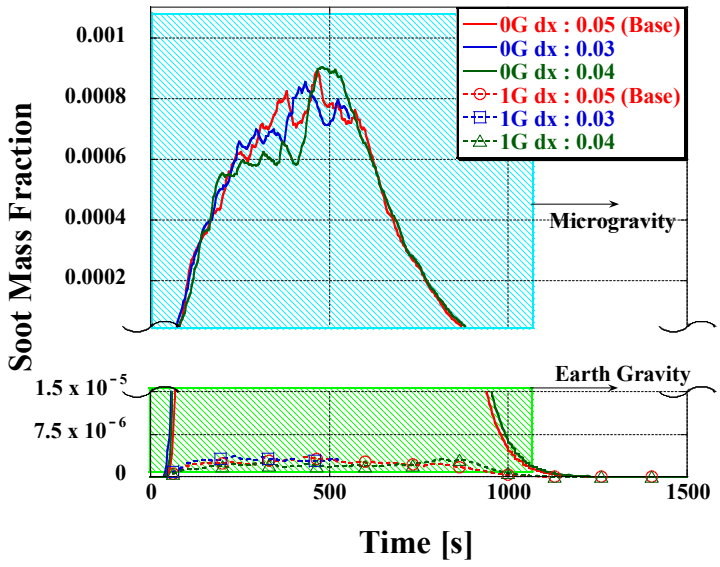

Figure 4. Sensitivity analysis of soot mass fraction calculated with different sizes of the mesh cell.

3. Results and Discussion

Figure 5 shows the calculated results of the ventilation flow inside the pressurized module by applying the boundary conditions listed in Table 2. The air diffuser and return register of the Destiny module are installed at a 45° angle with the walls of both sides (x–z plane), unlike the analysis model presented in Figure 5. Therefore, in the FDS computational analysis, the velocity vectors listed in Table 2 were used for the surfaces of the Air Diffuser and Return Register to form a pattern similar to the air circulation flow inside the Destiny module [11]. As can be seen in Figure 5, the rotational flow is generated by the air supply from three port (x–z plane) diffusers and three starboard (Stbd) diffusers, and a strong IMV flow is added to ensure fast and even ventilation throughout the module. The ventilation flow inside the pressurized module was almost uniform regardless of the change in gravity. It is important to address an issue related to the capability of the sub-grid models of turbulence in FDS in predicting the global effects of gravity and ventilation flow. NIST's efforts to validate the capability of FDS in response to addressed issues are well documented in previous investigations [25,26]. In those investigations, 1 g experimental data in the heating and ventilation literature which are close to conditions expected in low-gravity environments were used to verify the FDS performance to predict the air flow velocity profile. It was found that FDS predictions of the air flow velocities were in good agreement with the measurements.

Figures 6–9 show the mass fraction distribution of smoke particles, which was calculated using FDS by inputting the soot yields listed in Table 1 after positioning fire sources of the same size as the PVC and ABS samples used in the cone calorimeter experiment at the center of the Destiny module. As shown in these figures, the distribution of calculated mass fractions varies greatly depending on the gravity conditions with and without IMV flow. In particular, when an ABS fire source with a larger soot yield than that of PVC exists in the module, the mass fractions of smoke particles are highly and widely distributed under all conditions. As presented in Equation (5), the mass fraction and light extinction of smoke particles can directly influence the operation of a smoke detector. Based on the results obtained from the cone calorimeter experiment, the PVC fire can lower the mass fraction of smoke particles inside the module under the given flow condition owing to the lower soot yield than that of ABS fire. Furthermore, the low light extinction efficiency of the generated smoke particles may also affect the initial fire detection time.

As shown in Figure 6, the IMV flow in the pressurized module had the largest effect on the mass fraction distribution of smoke particles when PVC or ABS were burned in the microgravity environment. There is a limitation in moving the smoke particles from the fire source toward the smoke detector installed in the register return of the nadir (Earth) direction only by the rotational motion generated by the airflow supplied from the diffuser and discharged to the return register without IMV flow. Conversely, when the IMV was activated, which discharges much more flow than the airflow supplied from the diffuser, the mass fraction distribution of smoke particles improved. Particularly in the microgravity environment, the strong convective flow generated by the air density difference immediately after the occurrence of the fire is ignored, and the smoke particles move along the bottom of the nadir direction where the smoke detector is installed, mainly by the IMV flow. This implies that in the microgravity environment, the IMV flow can significantly affect the smoke detection performance.

Figures 6–9 show the calculation result of the smoke mass fraction distribution with and without IMV flow when the lunar (1.62 m/s^2), Mars (3.71 m/s^2), and Earth (9.81 m/s^2) gravities act inside the pressurized module under the same fire source (heat release rate, fire source position, and soot yield) and flow conditions for each fuel. The ABS fire source, which has a higher heat release rate than the PVC fire source, develops a larger buoyancy flow around it. Thus, as shown in these figures, the mass fraction distribution of the smoke particles inside the module is subjected to the dominant effect of buoyancy flow rather than ventilation flow, unlike in the microgravity environment. Particularly in the case of ABS, which has a higher heat release rate than PVC, the opposite result from Figure 6 can be seen as lunar gravity (1.62 m/s^2) is generated. First, buoyancy is generated by the temperature difference when the gravity field environment is formed and smoke particles concentrate in the upper layer. Furthermore, if there is strong IMV flow when the surroundings of the register are examined, it will hit the hatch wall and create an incidental flow opposite the wall, which will be evenly distributed. However, if there is no IMV flow, a relatively clear smoke mass fraction toward the register can be seen. In particular, when examining the smoke mass fraction results under Mars (Figure 8) and Earth (Figure 9) gravity, we can see that the buoyancy by the temperature difference is more prominent compared to that shown in Figure 6 owing to the relatively strong gravity field environment. Consequently, in the case of a fire in the gravity field environment, the flow by buoyancy that occurs along with the development of the flame will predominantly affect the movement of smoke particles and smoke detection performance.

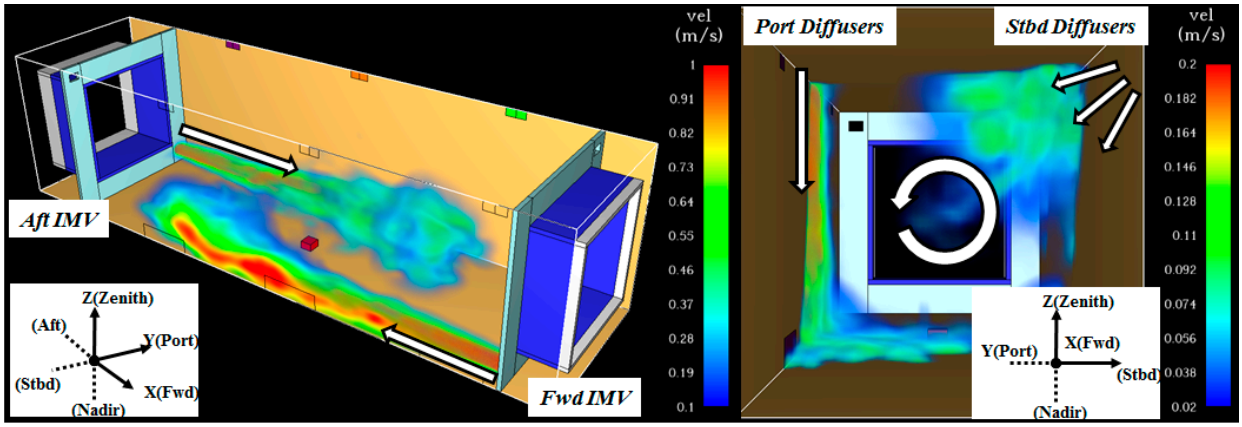

Figure 5. Ventilation flow inside ISS Destiny module numerically analyzed using FDS.

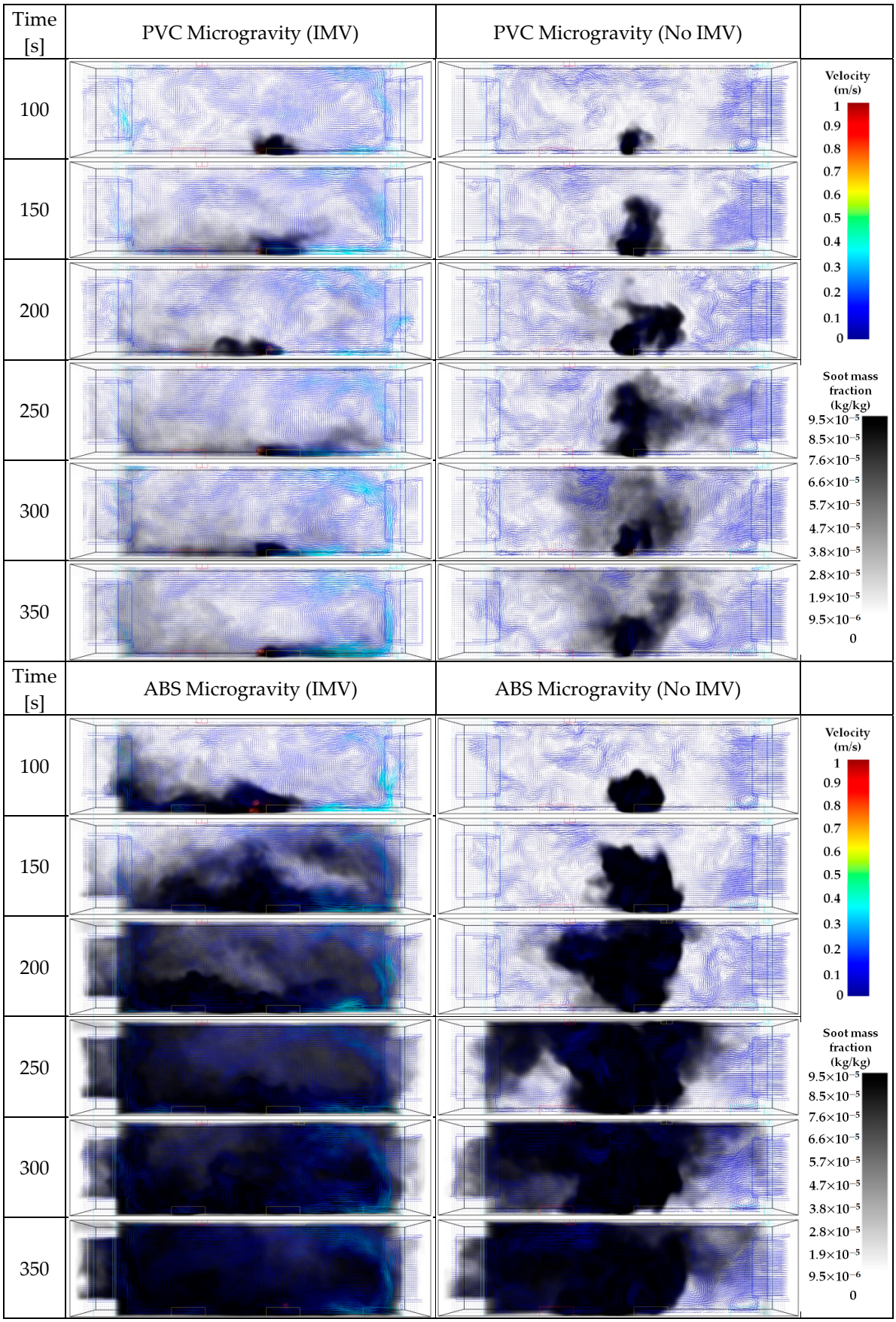

Figure 6. Smoke mass fraction with respect to time of PVC and ABS with and without IMV under microgravity.

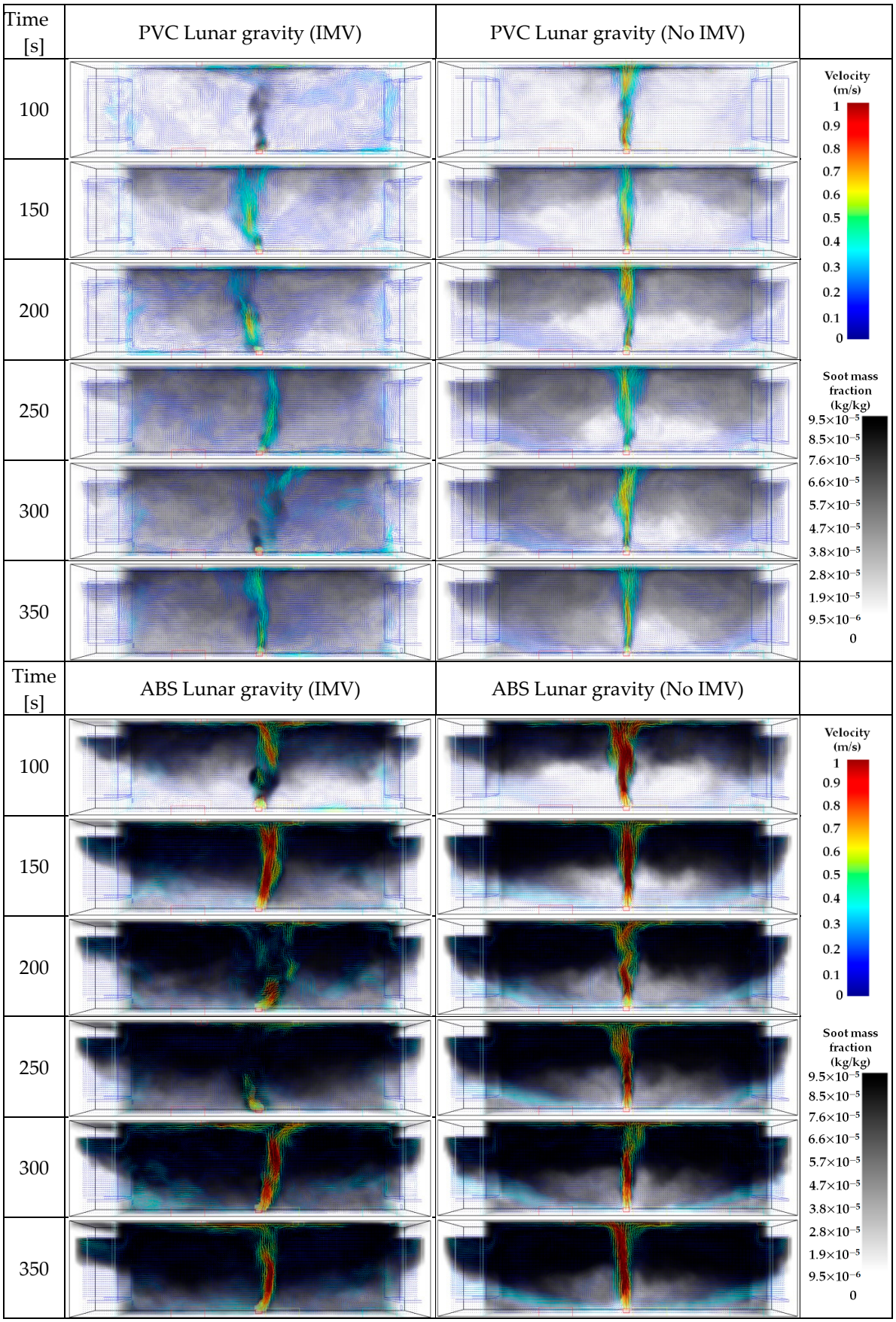

Figure 7. Smoke mass fraction with respect to time of PVC and ABS with and without IMV under lunar gravity.

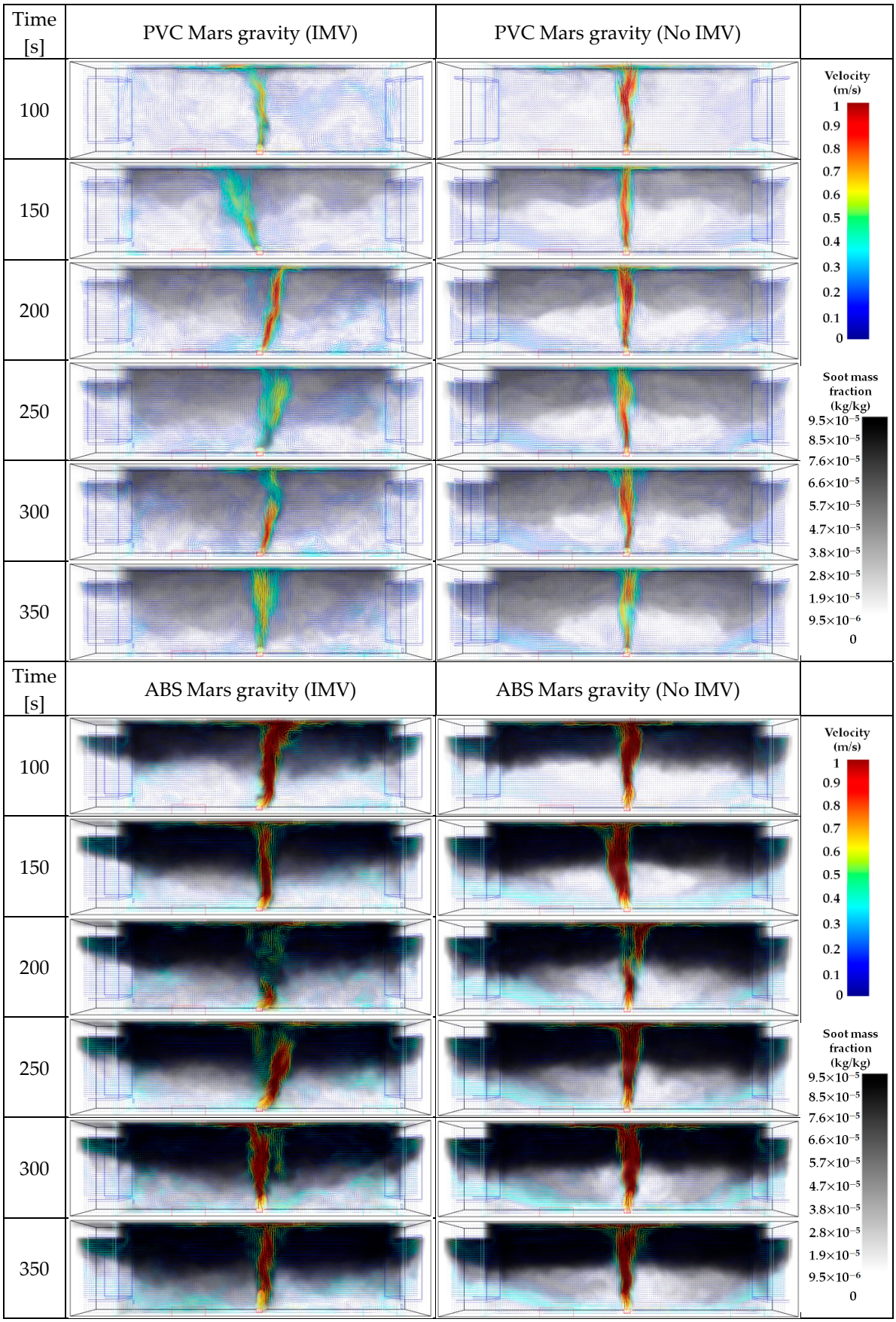

Figure 8. Smoke mass fraction with respect to time of PVC and ABS with and without IMV under Mars gravity.

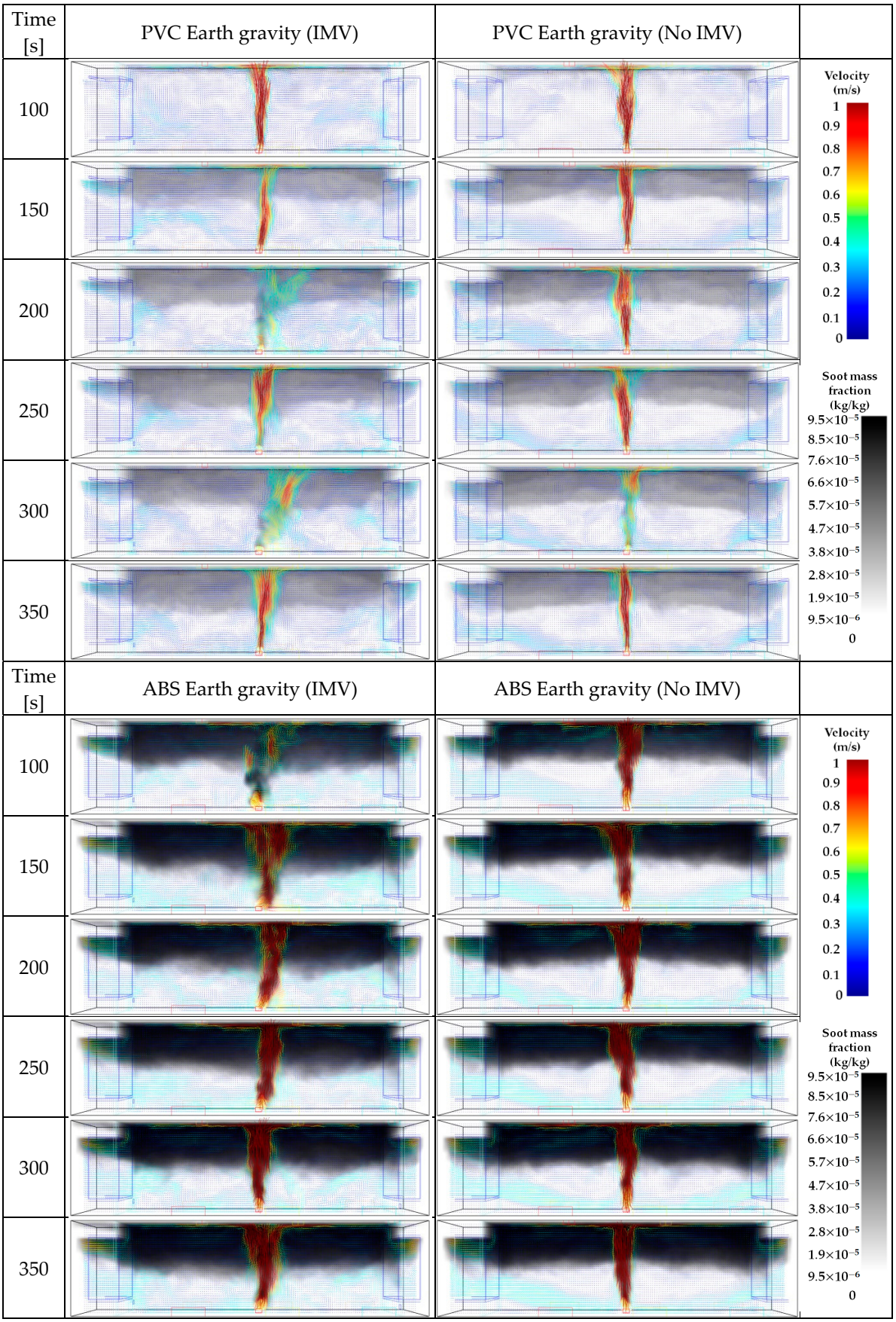

Figure 9. Smoke mass fraction with respect to time of PVC and ABS with and without IMV under Earth gravity.

Figure 10 shows a schematic of the smoke detector installed inside the Destiny module. The intensity of the light generated from the laser diode is monitored using two photodiodes, and a fire occurrence signal is transmitted by detecting the intensity of light, which is affected by smoke particles. However, to reduce malfunctions that can be caused by other particles such as dust, the intensity of light perpendicular to the photodiode sensor surface, and the intensity of light scattered at 30° are detected simultaneously, and the fire alarm signal is sent based on their ratio. The photoelectric smoke detector installed in the Destiny module is installed in almost all ISS modules except the pressurized module of the Russian side. Furthermore, this detector can detect particles of 0.3 μm at the minimum and is optimized for the detection of 1 μm or larger particles [8].

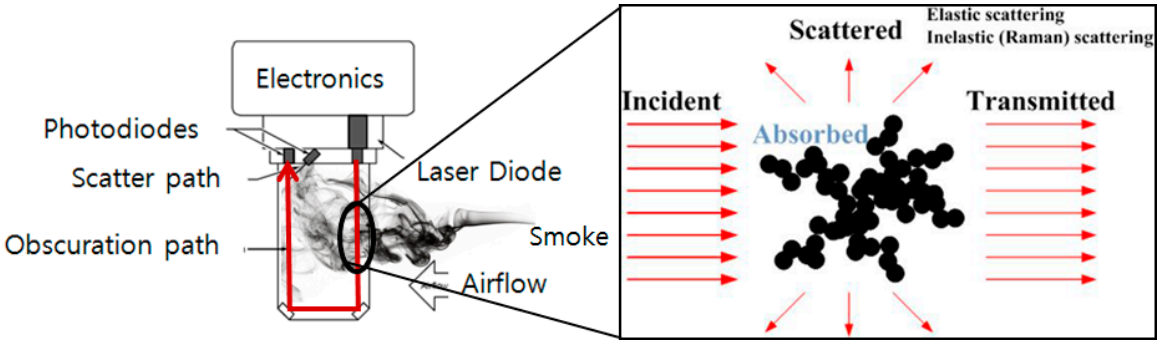

Figure 10. Schematic diagram of smoke detector installed onboard the Destiny module.

To detect the signals of smoke particles generated by a fire, the FDS provides a smoke detector function and generates alarm signals using a method similar to the abovementioned method. The soot mass fraction of each calculation grid is predicted based on the calculated flow field data and the input soot yield in proportion to the mass loss after ignition of the combustible, and the light transmittance ($\frac{I}{I_0}$) is calculated using Equation (11) in conjunction with the input mass extinction coefficient as follows:

$$\frac{I}{I_0} = \exp(-k_m \rho_{soot} y_{soot} L) \tag{11}$$

where $\rho_{soot} y_{soot}$ is the mass density of soot particles (g/m^3) and L is the path length. Because the light transmittance of Equation (11) changes with time, it can be expressed as the percent obscuration per meter (%/m) of the following Equation (12) [23,27]:

$$\mathrm{OPM} = \left(1 - \frac{I}{I_0}\right) \times 100 = \{1 - \exp(-k_m \rho_{soot} y_{soot}(t))\} \times 100 \tag{12}$$

Since $\rho_{soot} y_{soot}(t)$ is affected by the internal shape and flow of the detector, Equation (13), suggested by Cleary, was used to calculate the reaction and delay speed that can be caused by the shape or internal flow of the detector [23,27] as follows:

$$t_e = \alpha_e u^{\beta_e};\ t_c = \alpha_c u^{\beta_c},\ \Delta t = t_e + t_c \tag{13}$$

where t_e is the time when smoke particles flow into the detector, t_c is the time when smoke particles are mixed inside the detector, Δt is the response delay of the detector, u is the movement velocity of smoke particles, and α and β are the experience constants for considering the inflow and mixing of smoke particles, respectively. For calculation, α_c and β_c were set to 0.5 and −1.0, respectively, and the detector entry time was set to 0 (α_e = 0) [28]. The OPM was set to detect 3.28%/m [4].

Figures 11 and 12 show the smoke detection time when the OPM of the photoelectric smoke detector at each register was set to 3.28%/m when the combustibles of ABS and PVC were burned for each gravity in the cases of IMV flow (Figures 6–9). As

shown in Figures 11 and 12, the detection times of ABS and PVC in the microgravity match relatively well. This is because many smoke particles move toward the detector along with the IMV flow that acts relatively strongly near the bottom compared to the flow that circulates clockwise in the microgravity environment where buoyancy does not exist based on the development of flames. By contrast, as the gravity field environment in which buoyancy is generated incidentally increases, the detectors excluding LAP1RR and LAS5RR did not alarm (DNA). This is because in the case of a fire that occurs in the gravity field environment, the flow by buoyancy caused along with flame development has a dominant effect on the movement of smoke particles, and the IMV flow that is relatively strong on the bottom forms a flow field in the direction of each hatch and acts as a barrier. By contrast, in the case of LAP1RR and LAS5RR, it is believed that the IMV flow progresses in the direction of each hatch, and the smoke is detected when a strong IMV flow hits the hatch wall and generates an incidental flow at the other side of the wall.

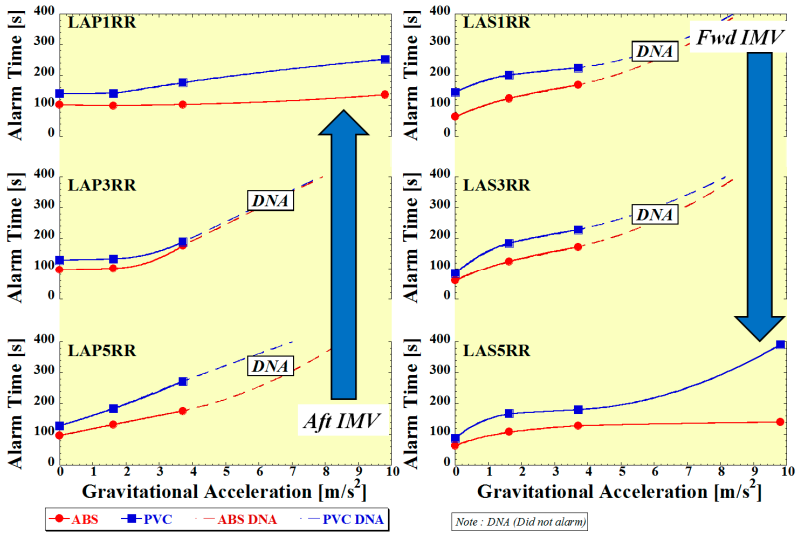

Figure 11. Detection time with respect to the gravity field environment of the smoke detector inside the Destiny module under IMV flow.

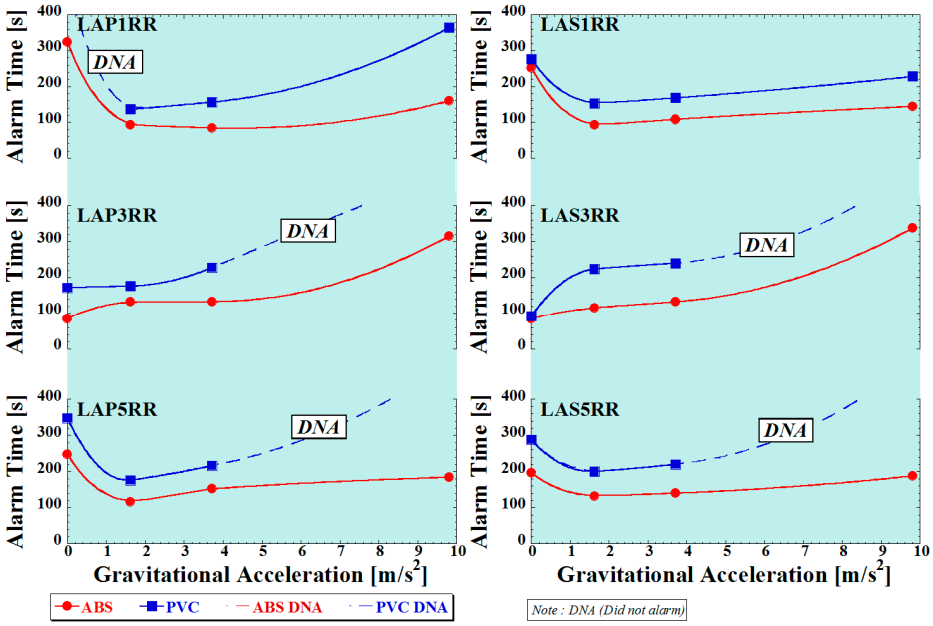

Figure 12. Detection time with respect to the gravity field environment of the smoke detector inside the Destiny module without IMV flow.

Figure 12 shows the case without IMV flow. In the microgravity environment, where buoyancy does not exist, the opposite result to the case with IMV flow is observed. If there was an IMV flow (Figure 11), the smoke detector issued alarm signals for approximately 100 s, whereas if there was no IMV flow, the smoke detection time increased by approximately 150 s in most cases except LAP3RR and LAS3RR, and the PVC combustible of LAP1RR became DNA. This is because most smoke particles move toward the smoke detector along with the IMV flow that becomes relatively strong near the bottom compared to the flow that circulates clockwise. By contrast, LAP3RR and LAS3RR, which have relatively fast detection times, can detect smoke because their distance to the combustible at the center of the Destiny module is short. Consequently, the ventilation flow plays a key role in smoke signal detection under microgravity, and the IMV flow, which is stronger than the clockwise ventilation flow, is a critical factor in shortening the overall smoke detection time. By contrast, as the gravity field environment in which buoyancy is generated increases, the detection of most smoke detectors of PVC with a lower smoke generation rate than that of ABS becomes DNA. This suggests that the fire of a combustible with a low smoke generation rate, such as PVC, may cause significant casualties because it is not detected by the smoke detector of the OPM (3.28%/m) currently set by the ISS. By contrast, the ABS with a high smoke generation rate shows opposite detection characteristics in the gravity field environment depending on the existence or absence of IMV flow. As mentioned above, a flow by buoyancy in the gravity field environment has a dominant effect on the movement of smoke particles, and the IMV flow that is relatively strong on the bottom serves as a barrier. When there is no IMV flow to act as a barrier, the smoke is detected by the effect of the diffuser and register flows, which are relatively distinct. In other words, the fire that occurs in the gravity field environment is dominated by the flow caused by buoyancy, and the IMV flow for ventilation does not help detect smoke particles.

4. Conclusions

This study derived the information of combustibles (MLR, heat of combustion, thermal properties) by conducting the ISO 5660-1 cone calorimeter experiment for PVC used in electrical wires and ABS used in PCs and monitors in a real manned exploration module under Earth gravity. Furthermore, numerical modeling of FDS was conducted by linking the smoke behavior and detection characteristics of ABS and PVC with the ventilation flow condition depending on the change in the gravity field for the Destiny module, a U.S. pressurized module of the ISS. The conclusions of this study are as follows:

1. The smoke behavior in the microgravity environment was distinctly different from that in the gravity field environment, as the buoyancy was gone. In the gravity field environment, the circulation flow inside the module did not significantly affect the smoke detection time. Conversely, it delayed the detection because the IMV flow, which is relatively strong at the bottom, served as a barrier.
2. By contrast, in the microgravity environment, the ventilation flow played a crucial role in detecting smoke signals. In particular, the IMV flow, which is stronger than the clockwise ventilation flow, was a crucial factor in shortening the overall smoke detection time.
3. In the case of a fire that occurred in the gravity field environment, the flow by buoyancy that was generated along with the development of flames had a dominant impact on the movement of smoke particles. Furthermore, buoyancy appeared more prominently as the gravity increased. Consequently, the design needs to consider selecting the smoke detector position and internal flow based on the gravity condition.
4. In the case of PVC with a lower smoke generation rate than ABS, the smoke detection performance has significantly deteriorated. In the manned exploration module, there is a possibility of significant casualties because the smoke detector of the OPM (3.28%/m) currently set on the ISS cannot detect smoke. Thus, the OPM of the smoke detector should be set appropriately depending on the combustible.

The selection of the detector's position and the detection time with respect to the gravity environment can vary greatly depending on the fire source and internal flow. Hence, computational or experimental studies should be conducted considering these factors. The findings of this study will provide basic data for the design of the fire detection system for manned space exploration modules.

Author Contributions: S.-H.P. provided the main idea of the study; T.-K.H. designed and performed the experiments; T.-K.H. wrote the original draft; S.-H.P. reviewed and edited the draft. All authors have read and agreed to the published version of the manuscript.

Funding: This research was supported by the Korea Aerospace Research Institute (Award Number 171111560), and "Human Resources Program in Energy Technology" of the Korea Institute of Energy Technology Evaluation and Planning (KETEP) granted financial resource from the Ministry of Trade, Industry & Energy, Republic of Korea (No. 20194030202410).

Institutional Review Board Statement: Not applicable.

Informed Consent Statement: Not applicable.

Data Availability Statement: Not applicable.

Conflicts of Interest: The authors declare no conflict of interest. The funders had no role in the design of the study; in the collection, analyses, or interpretation of data; in the writing of the manuscript, or in the decision to publish the results.

References

1. Kauffman, J. Adding Fuel to the Fire: NASA's Crisis Communications Regarding Apollo 1. *Public Relat. Rev.* **1999**, *25*, 421–432. [CrossRef]
2. Ruff, G.A.; Urban, D.L.; King, M.K. A Research Plan for Fire Prevention Detection and Suppression, AIAA-2005-0341. In Proceedings of the 43rd Aerospace Sciences Meeting and Exhibit, Reno, NV, USA, 9–12 January 2005. [CrossRef]
3. Urban, D.L.; Ruff, G.A.; Brooker, J.; Cleary, T.; Yang, J.C.; Mulholland, G.W.; Yuan, Z.G. Spacecraft Fire Detection: Smoke Properties and Transport in Low-Gravity. In Proceedings of the 46th AIAA Aerospace Sciences Meeting and Exhibit, Reno, NV, USA, 7–10 January 2008.
4. Brooker, J.E.; Urban, D.L.; Ruff, G.A. ISS Destiny Laboratory Smoke Detection Model. In Proceedings of the 37th International Conference on Environmental Systems (ICES), Chicago, IL, USA, 9–12 July 2007. [CrossRef]
5. Ross, H.D.; Gokoglu, S.A.; Friedman, R. *Microgravity Combustion Science: 1995 Program Update*; NASA Technical Memorandum; NASA: Washington, DC, USA, 1995; p. 106858.
6. Bukowski, R.W.; Mulholland, G.W. *Smoke Detector Design and Smoke Properties*; Dept. of Commerce, National Bureau of Standards, National Engineering Laboratory, Center for Fire Research: Washington, DC, USA, 1978.
7. Wang, X.; Zhou, H.; Arnott, W.P.; Meyer, M.E.; Taylor, S.; Firouzkouhi, H.; Moosmüller, H.; Chow, J.C.; Watson, J.G. Characterization of smoke for spacecraft fire safety. *J. Aerosol Sci.* **2019**, *136*, 36–47. [CrossRef]
8. Urban, D.L.; Ruff, G.A.; Cleary, T.; Yang, J.; Molholland, G.; Yuan, Z. Detection of Smoke from Microgravity Fire. In Proceedings of the 35th International Conference on Environmental Systems (ICES), Rome, Italy, 11–14 July 2005. [CrossRef]
9. Schultze, T.; Sichma, L.; Meyer, M. A Smoke Detector to Prevent False Alarms in Lunar Missions by Smoke-Dust Discrimination. In Proceedings of the 50th International Conference on Environmental Systems (ICES), Lisbon, Portugal, 12–16 July 2020.
10. Meyer, M.E.; Urban, D.L.; Mulholland, G.W.; Bryg, V.; Yuan, Z.-G.; Ruff, G.A.; Cleary, T.; Yang, J. Evaluation of spacecraft smoke detector performance in the low-gravity environment. *Fire Saf. J.* **2018**, *98*, 74–81. [CrossRef] [PubMed]
11. Mulholland, G.W.; Meyer, M.; Urban, D.L.; Ruff, G.A.; Yuan, Z.-G.; Bryg, V.; Cleary, T.; Yang, J. Pyrolysis Smoke Generated Under Low-Gravity Conditions. *Aerosol Sci. Technol.* **2015**, *49*, 310–321. [CrossRef]
12. Meyer, M.E.; Mulholland, G.W.; Bryg, V.; Urban, D.L.; Yuan, Z.-G.; Ruff, G.A.; Cleary, T.; Yang, J. Smoke Characterization and Feasibility of the Moment Method for Spacecraft Fire Detection. *Aerosol Sci. Technol.* **2015**, *49*, 299–309. [CrossRef]
13. Urban, D.L.; Ruff, G.A.; Mulholland, G.W.; Cleary, T.G.; Yang, J.C.; Yuan, Z. Measurement of Smoke Particle Size under Low-Gravity Conditions. *SAE Int. J. Aerosp.* **2008**, *1*, 317–324. [CrossRef]
14. Lyon, R.E.; Janssens, M.L. *Polymer Flammability*; Report No.: DOT/FAA/AR-05/14; Federal Aviation Administration: Springfield, VA, USA, 2005.
15. Shemwell, B.E.; Levendis, Y.A. Particulates Generated from Combustion of Polymers (Plastics). *J. Air Waste Manag. Assoc.* **2000**, *50*, 94–102. [CrossRef] [PubMed]
16. Günther, M.; Lorenzetti, A.; Schartel, B. Fire Phenomena of Rigid Polyurethane Foams. *Polymers* **2018**, *10*, 1166. [CrossRef] [PubMed]
17. Twilley, W.H.; Babrauskas, V. *User's Guide for the Cone Calorimeter*; NBS Special Publication 745; Government Printing Office: Washington, DC, USA, 1998.

18. Tsantaridis, L. *Smoke, Gas and Heat Release Data for Building Products in the Cone Calorimeter*; Rapport 1 8903013; Institutet för Träteknisk Forskning (Trätek): Stockholm, Sweden, 1989.
19. Hong, T.-K.; Roh, B.-S.; Park, S.-H. Measurements of Optical Properties of Smoke Particulates Produced from Burning Polymers and Their Implications. *Energies* **2020**, *13*, 2299. [CrossRef]
20. Guyot, A.; Bert, M.; Michel, A. Smoke reduction from polyvinyl chloride (PVC). *Fire Saf. J.* **1983**, *5*, 287–297. [CrossRef]
21. Wang, Z.; Huang, P.; Fan, W.C.; Wang, Q. Measurements on the Fire Behaviour of PVC Sheets using the Cone Calorimeter. *Fire Saf. Sci.* **1988**, *3*, 221–228.
22. McGrattan, K.; Hostikka, S.; McDermott, R.; Floyd, J.; Weinschenk, C.; Overholt, K. *Fire Dynamic Simulator User's Guide*, 6th ed.; NIST Special Publication 1019; NIST: Gaithersburg, MD, USA, 2017. [CrossRef]
23. McGrattan, K.; Hostikka, S.; Floyd, J.; McDermott, R.; Vanella, M. *Fire Dynamics Simulator Technical Reference Guide Volume 1: Mathematical Model*, 6th ed.; NIST Special Publication 1018-1; NIST: Gaithersburg, MD, USA, 2021. [CrossRef]
24. Son, C.H.; Evgueni, M.S.; Nikolay, G.I.; Denis, S.T. Integrated Computational Fluid Dynamics Ventilation Model for the International Space Station. In Proceedings of the 35th International Conference on Environmental Systems (ICES), Rome, Italy, 11–14 July 2005.
25. Linteris, G.T. *Large Scale Fire Dynamics in Spacecraft in Reduced Gravity*; NIST NNC04IA17I; NIST: Gaithersburg, MD, USA, 2011.
26. Musser, A.; McGrattan, K.B.; Palmer, J.M. *Evaluation of a Fast, Simplified Computational Fluid Dynamics Model for Solving Room Airflow Problems*; NISTIR 6760; NIST: Gaithersburg, MD, USA, 2001.
27. Cleary, T.; Chernovsky, A.; Grosshandler, W.; Anderson, M. *Particulate Entry Lag in Spot-Type Smoke Detectors*; International Association for Fire Safety Science (IAFSS): London, UK, 1999; Volume 263, pp. 779–790.
28. Roby, R.J.; Klassen, M.S.; Zhang, W.; Olenick, S.M.; Gaines, G. *Development of an Algorithm for Modeling of ISS and Shuttle Smoke Detector Activation in Forced Flow Ventilation Environments Using Fire Dynamics Simulator*; Combustion Science & Engineering: Columbia, MD, USA, 2005.